Utilizing Core–Shell Fibrous Collagen-Alginate Hydrogel Cell Delivery System for Bone Tissue Engineering

Roman A. Perez, PhD,[1] Meeju Kim, BSc,[1,2] Tae-Hyun Kim, PhD,[1,2] Joong-Hyun Kim, PhD,[1,2]
Jae Ho Lee, PhD,[1,2] Jeong-Hui Park, BSc,[1,2] Jonathan C. Knowles, PhD,[1,3] and Hae-Won Kim, PhD[1,2,4]

Three-dimensional matrices that encapsulate and deliver stem cells with defect-tuned formulations are promising for bone tissue engineering. In this study, we designed a novel stem cell delivery system composed of collagen and alginate as the core and shell, respectively. Mesenchymal stem cells (MSCs) were loaded into the collagen solution and then deposited directly into a fibrous structure while simultaneously sheathing with alginate using a newly designed core–shell nozzle. Alginate encapsulation was achieved by the crosslinking within an adjusted calcium-containing solution that effectively preserved the continuous fibrous structure of the inner cell-collagen part. The constructed hydrogel carriers showed a continuous fiber with a diameter of ~700–1000 μm for the core and 200–500 μm for the shell area, which was largely dependent on the alginate concentration (2%–5%) as well as the injection rate (20–80 mL/h). The water uptake capacity of the core–shell carriers was as high as 98%, which could act as a pore channel to supply nutrients and oxygen to the cells. Degradation of the scaffolds showed a weight loss of ~22% at 7 days and ~43% at 14 days, suggesting a possible role as a degradable tissue-engineered construct. The MSCs encapsulated within the collagen core showed excellent viability, exhibiting significant cellular proliferation up to 21 days with levels comparable to those observed in the pure collagen gel matrix used as a control. A live/dead cell assay also confirmed similar percentages of live cells within the core–shell carrier compared to those in the pure collagen gel, suggesting the carrier was cell compatible and was effective for maintaining a cell population. Cells allowed to differentiate under osteogenic conditions expressed high levels of bone-related genes, including osteocalcin, bone sialoprotein, and osteopontin. Further, when the core–shell fibrous carriers were implanted in a rat calvarium defect, the bone healing was significantly improved when the MSCs were encapsulated, and even more so after an osteogenic induction of MSCs before implantation. Based on these results, the newly designed core–shell collagen-alginate fibrous carrier is considered promising to enable the encapsulation of tissue cells and their delivery into damaged target tissues, including bone with defect-tunability for bone tissue engineering.

Introduction

TISSUE ENGINEERING has great promise as a strategy to enable regeneration of damaged or injured tissues, including bone. As the key component, scaffolds play critical roles in supporting cells in the initial adhesion, migration, and proliferation. Among the cell sources, stem cells offer great opportunities for regenerative therapy due to their self-renewal and proliferative potential and the possible lineage commitment under defined conditions.[1,2] Whereas the delivery of stem cells to damaged tissues is considered promising, it has remained difficult to maintain a high survival rate of cells under biological conditions associated with pH, temperature, oxygen tension, and nutrient diffusion, thus

requiring a protected delivery. Further, stem cells need to be given appropriate cues, such as signaling molecules, mechanical stiffness, or material composition to induce proper cell differentiation and significant tissue regeneration in vivo.[3–5] A system that is both simple and reproducible, which can be used either in the laboratory to pass to the surgical room or directly during surgery, is also important.

Cell encapsulation has been shown to be an efficient delivery system capable of protecting stem cells from the surrounding tissues, while providing appropriate microenvironments for survival and differentiation. Hydrogel biopolymers such as collagen, alginate, and chitosan have shown cellular compatibility and the capacity to load and carry cells to the target tissues.[5–8] Collagen can load cells and has good

[1]Institute of Tissue Regeneration Engineering (ITREN), [2]Department of Nanobiomedical Science and WCU Research Center, and [4]Department of Biomaterials Science, College of Dentistry, Dankook University, Cheonan, South Korea.
[3]Biomaterials and Tissue Engineering, University College London Eastman Dental Institute, London, United Kingdom.

biocompatibility, while maintaining cellular functions that mimic the native three-dimensional (3D) tissue environment.[9] Collagen also becomes a gel when pH, ionic concentration, and temperature are modulated to near biological conditions.[10] However, despite its excellent biocompatibility, it is very difficult to adjust the collagen hydrogels into various shapes for tissue defect sites, while maintaining the hydrogel form.

As an alternative, alginate can be used to load tissue cells within the structure and subsequently deliver them into the defect site.[11–13] When compared to other types of natural polymer hydrogels such as collagen, alginate has a major advantage in that it does not disintegrate when placed in aqueous media and therefore may retain the initial shape also allowing to be formulated into different shapes, including microspheres and fibers.[14] This is because alginate possesses the useful property of undergoing crosslinking when placed in contact with divalent ions, such as calcium (Ca^{2+}),[15] thus allowing for maintenance of the shape. Nevertheless, its biological properties are poor in terms of cell adhesion, migration, and viability, and thus, it has usually been combined with other natural polymers or specific sequences such as arginin-glycin-aspartic acid (RGD) to enhance the cell survival rate.[16]

We aimed to develop a system that utilizes the best properties of alginate and collagen, and to develop a simple process allowing the extrusion of large volumes of encapsulated cells. A novel structured cell delivery system was developed based on a hydrogel consisting of the collagen inner core and alginate outer shell, whereby cells are loaded and delivered in the collagen inner part. Specifically, the core–shell hydrogel cell delivery system was produced in a fibrous structure using a simple robotic dispensing machine, which we have previously used as a dual drug delivery system.[17] Deposition of fibers was made through the concentric nozzle into an adjusted Ca^{2+}-containing bath. The crosslinking of alginate aided the structural stability, while maintaining the shape of the collagen core. The processing tools used to generate the novel core–shell structured collagen-alginate hydrogel carriers are described, and the viability and proliferation of mesenchymal stem cells (MSCs) within the hydrogel carriers as well as their osteogenic potential *in vitro* under defined biochemical cues were investigated. Finally, the ability to deliver MSCs *in vivo* and their new bone formation were addressed in a rat calvarium model, which may provide useful information on the use of the system in delivering stem cells for bone tissue engineering.

Materials and Methods

Core–shell fiber processing

A dual concentric nozzle (inner 23G and outer 17G) was specifically designed and used to produce a core–shell structured fibrous network of collagen-alginate. The sodium alginate used (A2158; Sigma-Aldrich) had an M/G ratio of 1.67 and a molecular weight of ∼50,000 Da. Solutions of sodium alginate at ratios of 2%–5% (% wt) in water were fed into the outer syringe, while the collagen solution was loaded in the inner syringe. The schematic representation is shown in Figure 1a. The collagen (rat tail type I collagen; First Link; 2.05 mg/mL) solution was prepared by mixing 1 mL of collagen with 100 μL of 10× Dulbecco's modified Eagle medium and a proper amount of 1 N sodium hydroxide to provide a neutral pH to adjust solution conditions for subsequent gelation and providing a nontoxic

environment for the loaded cells. Each syringe was attached to an injection pump (KD Scientific) connected through a microtube and the injection rate varied between 20 and 80 mL/h. Core–shell structured collagen-alginate fibers were then injected through the concentric nozzle into a bath containing 50 mM calcium chloride $(CaCl_2)$ for 5 min. The whole injection process was performed under sterile conditions. Following injection, the outer alginate was in contact with the calcium ions, which resulted in crosslinking and gelation to maintain the stability of the fibrous cell carrier.

Characterizations of core–shell hydrogels

After deposition of the core–shell fibrous structure, the thickness of the core and shell was measured from 10 arbitrarily selected images obtained by optical microscopy. Fibrous hydrogel samples prepared with varying injecting speed (20, 50, and 80 mL/h) or alginate concentration (2%, 3%, and 5%) were used for the measurement. The mechanical properties of the fibrous hydrogels were measured by dynamic mechanical analysis (DMA; MetraVib, DMA25N) using a parallel plate configuration. For this, the deposited fibers were stacked into a cylindrical Teflon mould (12 mm diameter × 6 mm height) at a constant volume (0.5 mL of sample). Mechanical testing was carried out using dynamic frequency sweep with frequencies ranging from 0.1 to 10 Hz at 37°C and with strain amplitude of 5%, which was in the linear region of viscoelasticity. Both auto-compression and auto-strain adjustment were applied. The force was ramped from 0.001 to 0.2 N and the maximum allowed strain was set at 10%. The storage modulus (E') and loss modulus (E'') of the samples were measured. The phase angle delta (tan delta) was computed as E''/E' ($n=3$).

The water uptake capacity of the fibrous hydrogel cell carriers was assessed. After immersion of each sample in distilled water for 1 h, the sample was taken out and blotted on a filter paper saturated with distilled water, and the weight was recorded (W_{im}). After washing and freeze drying the sample, the dried weight was recorded (W_{dry}). The water uptake capacity was determined as $(W_{im} - W_{dry})/W_{dry}$ and was expressed as percentage ($n=3$). Degradation of the samples (0.3 mL for each sample) was tested by immersion of each sample in phosphate-buffered saline (PBS) ($n=3$). After immersion for various time periods up to 21 days, the sample was obtained, washed, and dried, and the weight after the degradation test was recorded (W_{deg}). The degradation rate was considered as the percentage of $(W_{dry} - W_{deg})/W_{dry}$.

Cell isolation

MSCs derived from rat bone marrow were harvested from the femora and tibiae of adult rats (180–200 g) according to the guidelines approved by the Animal Ethics Committee of Dankook University. The harvested product was centrifuged and the supernatant was collected and suspended within a culture flask containing a normal culture medium; the α-minimal essential medium (α-MEM) supplemented with 10% fetal bovine serum (FBS) and 100 U/mL penicillin and 100 mg/mL streptomycin in a humidified atmosphere of 5% CO_2 in air at 37°C. After incubation for 1 day, the medium was refreshed and cultured until the cells reached near confluence. The cells were subcultured by trypsin and
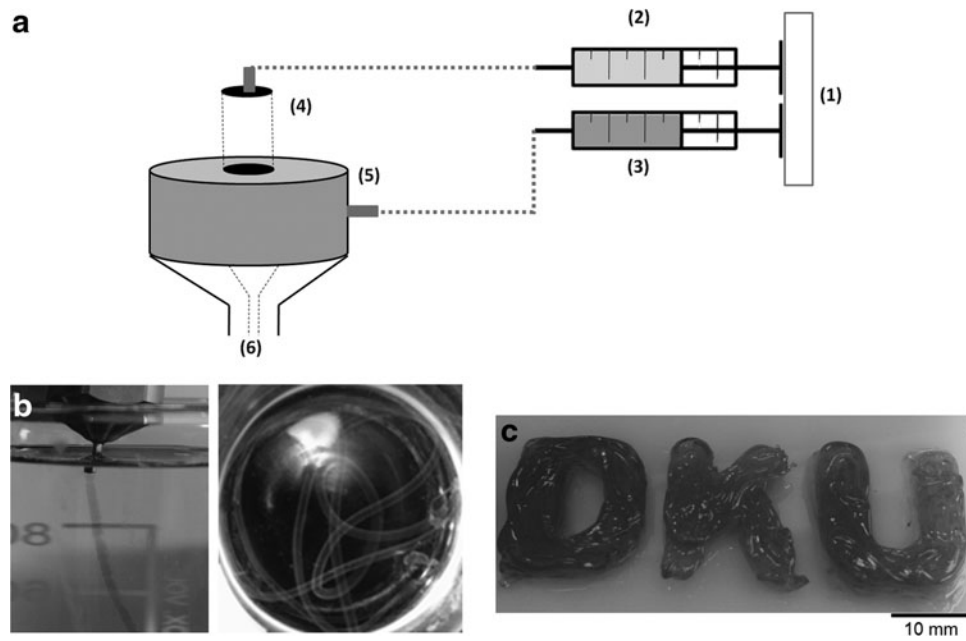
FIG. 1. Schematic showing the equipment setup for producing the stem cell-loaded collagen core and alginate shell hydrogel carrier. **(a)** Each solution of mesenchymal stem cell (MSC) collagen (2) and alginate (3) was advanced at a constant speed from injectors (1), which were directly deposited using the core–shell needle (4, 5) designed for this study under a low concentration (50 mM) of calcium chloride solution bath (6), during which time the alginate was allowed to harden through crosslinking of the Na-alginate with the Ca ion. The MSCs loaded within the collagen inner core became encapsulated within the hardened alginate. The direct deposited cell construction was subsequently incubated at 37°C to allow the gelation of collagen, after which, it was further incubated for cell cultivation for bone tissue engineering. **(b)** Deposited core–shell hydrogel carrier preserving a continuous fiber structure. **(c)** Core–shell fibrous hydrogel carrier is easily molded into any determined shape (letter *DKU* replicated as an example), tuning to the tissue-defect geometry.

maintained in the normal culture condition. Cells at two to three passages were used for further tests.

Cell encapsulation

For cell encapsulation, sodium alginate powder was sterilized with ethylene oxide and then preserved under sterile conditions. The powder was mixed with distilled water to produce 3% sodium alginate solutions. The collagen solutions in product were in sterile conditions and were used as received. To incorporate MSCs in the collagen hydrogel, the collagen hydrogel was prepared as previously described, incorporating 1×10^5 cells after the pH reached a neutral value, which was observed by the color change of the collagen solution (from yellow to orange-pink). The cell-loaded collagen solution was put in the inner syringe, whereas the alginate solution was in the outer syringe, and a fibrous structuring was performed in sterile conditions as described above. The amount of collagen present in the core–shell fiber structure was maintained at 0.3 mL for all cases ($n = 3$). As a result, a cell-encapsulated fibrous hydrogel (cell-collagen in the core and alginate in the shell) was obtained. After scaffold construction for 5 min, the cell-encapsulated hydrogel was washed with a culture medium three times to remove the excess $CaCl_2$, and then cultured in the α-MEM containing 10% FBS and 1% penicillin/streptomycin in a humidified incubator at 37°C under 5% CO_2 for up to 21 days. As the positive control group, 0.3 mL of collagen hydrogel containing 1×10^5 MSCs was molded in a culture well without the core–shell fibrous structuring ($n = 3$).

Confirmation of cell viability and growth

The number of viable cells in the core–shell fibrous cell carrier or in the collagen gel was measured. At each culture period, hydrogel samples containing cells were washed with PBS twice and dissolved with 1% type I collagenase (Sigma) for 5 min at 37°C. The suspension was then centrifuged to remove the supernatant and the number of viable cells was quantified by Trypan blue screening and using a hemocytometer. The cell proliferative potential was measured using the double-stranded DNA detection kit (Quanti-iT Picogreen; Invitrogen). For this, the hydrogels incorporating cells were washed and dissolved with 1% type I collagenase (Sigma). After collecting the cell pellet, the samples were stored at -20°C. The mixture was then freeze–thawed by two repeating cycles. The cells were quantified according to the manufacturer's specifications by measuring the fluorescence intensity at an excitation of 485 nm and emission of 530 nm. A standard curve was also made according to the manufacturer's instructions and was used for converting fluorescence intensity to DNA content.

Observation of cell morphology

The cell morphology was monitored under light microscopy using an Olympus BX-50 microscope during culture. At each culture period (7, 14, and 21 days), the cells grown on each sample were fixed with 4% paraformaldehyde and then treated with 0.1% Triton X-100. After washing with PBS, Alexa Fluor 546-conjugated phalloidin (Invitrogen A22283)

diluted in PBS was added to each sample to stain the F-actin. A ProLong Gold antifade reagent with 4′,6-diamidino-2-phenylindole (Invitrogen) was used to stain the cells and produce blue fluorescence upon binding to the DNA in the nucleus, after which, images were obtained by confocal laser scanning microscopy using a Zeiss LSM 510 microscope.

Determination of cell differentiation by quantitative polymerase chain reaction

MSCs encapsulated within the hydrogel cell carrier were induced to osteogenic differentiation in an osteogenic medium containing 50 μg/mL ascorbic acid, 10 mM β-glycerol phosphate, and 10 nM dexamethasone. Gene expression associated with osteogenesis, including osteocalcin (OCN), bone sialoprotein (BSP), and osteopontin (OPN), was assessed by quantitative polymerase chain reaction (qPCR). After culture for 14 and 21 days, the cell-loaded scaffolds were washed and then dissolved with collagenase. The cell pellet was collected and frozen at −80°C until used. Total RNA was extracted from differentiated cells using the RNeasy Kit (Qiagen) according to the manufacturer's instructions. The concentration of RNA samples was quantified using a Nanodrop 2000 spectrophotometer (Thermo Scientific). RNA samples were transcribed into cDNA by combining the RNA with random hexamer, followed by denaturation at 70°C for 5 min. After denaturation, the samples were mixed with the reverse transcription (RT) premix for complete cDNA synthesis. cDNA was then amplified using RT-PCR premix (Bioneer) at 94°C for 5 min, followed by 35 cycles of 94°C for 1 min denaturation, 57°C for 1 min for annealing, and 72°C during 1 min for extension. Primers used for amplification were OCN: AGGACCCTCT CTCTGCTCAC (forward), AACGGTGGTGCCATAGATGC (reverse); BSP: CTGCTTTAATCTTGCTCTG (forward), CCA TCTCCATTTTCTTCC (reverse); OPN: TCCAGCTGACTTG ACTCATGG (forward), CCGATGAATCTGATGAGTCCTT (reverse); and glyceraldehyde-3-phosphate dehydrogenase (GAPDH): CCATGTTTGTGATGGGTGTG (forward), GGAT GCAGGGATGATGTTCT (reverse). Results were normalized with respect to GAPDH.

In vivo delivery in rat calvarium defect

Tissue compatibility and the bone forming ability of the MSCs delivering hydrogel cell carriers were assessed using a rat calvarium defect model. The protocol of the housing, care, and experimental protocol was approved by the Dankook University Institutional Animal Care and Use Committee, Korea. Nine 11-week-old, 350–400 g healthy male Sprague-Dawley rats were used. During the surgical operation, the animals were anesthetized with intramuscular injections of 80 mg/kg zoletil and 10 mg/kg xylazine in the right quadriceps muscle. All instruments were sterilized before the procedures and all the surgical procedures on animals were carried out under general anesthesia using sterile techniques. Following a midline incision through the skin and the excision of the periosteum using a No. 10 blade with a Bard–Parker scalpel, the cranial bone was exposed. A 5-mm diameter, full-thickness cylindrical defect was created at the midportion of each parietal bone by means of a trephine burr. Two defects were created on each animal, and the defects were randomized into three groups. The defect was filled with 0.1 mL of test sample. Group 1 consisted of the cell carrier only. Group 2 comprised the cell carrier encapsulating nondifferentiated MSCs. Group 3 contained the cell carrier encapsulating differentiated MSCs ($n = 4$). For group 3, the MSCs in the hydrogel construct were cultured under an osteogenic medium for one week. After the implantation, the subcutaneous area was sutured with 4-0 absorbable suture material, and the skin was subsequently sutured with 4-0 non-absorbable monofilament suture material. After surgery, the rats were housed individually in cages under conditions at 20°C–24°C and 30%–70% relative humidity and kept on an alternating 12-h light/12-h dark cycle with standard pellet food and water provided *ad libitum*. Animals were monitored for signs of infection, inflammation, and adverse effects by visual observation for one week.

Analyses of bone regeneration

At 6 weeks postoperatively, the animals were sacrificed for harvesting of the samples and surrounding tissues. The specimens were harvested from each animal at the time of euthanasia and fixed in 10% of neutral buffered formaldehyde solution for at least 24–48 h. The samples were imaged using a high-resolution microcomputed tomography (μCT) system (Skyscan 1072; Skyscan) to evaluate tissue recovery and bone regeneration. The harvested samples were scanned and serial coronally oriented tomograms were reconstructed from the raw images using NRecon CT Reconstruction software. A cylindrical region of interest (ROI) was precisely positioned over the center of each defect, encompassing all new bone within the defect site. Coronally oriented μCT images were then reformatted in an axial orientation. Reconstructed images over the ROI using a CTAn (Skyscan) and 3D images were created. The total volume of newly formed bone within each ROI was measured by assigning a threshold for the total bone content (including trabecular and cortical bone). Bone surface area and surface density were also recorded. Four samples for each group were measured and the total volume of bone is reported (mm^3).

After μCT scanning, specimens were decalcified with the RapidCal™ solution and dehydrated in a graded series of increasing ethanol concentrations (70%–100%), and then trimmed and embedded in paraffin. Tissue sections ∼5 μm in thickness were prepared perpendicular to the cranial bone and the sections were stained with hematoxylin–eosin (HE) and Masson's trichrome (MT) for histopathological examination to check biocompatibility and bone formation. Light microscopy digital images were obtained using Meta-Morph and analyzed with computerized image analysis system (Molecular Devices).

Statistical analysis

Experiments were performed in triplicate, unless otherwise specified. Data are expressed as mean ± one standard deviation. Statistical analysis was carried out by one-way analysis of variance with the Fisher's *post hoc* test and the significance level was considered at $p < 0.05$ or $p < 0.01$.

Results

Generation of core–shell hydrogel cell carriers and properties

Using the device (depicted in Fig. 1a), core–shell structured hydrogel cell carriers could be produced. The core–shell fibrous injection through the co-concentric nozzle and

the gathering of fibrous scaffolds were optically visualized (Fig. 1b). A continuous fiber preserving the core–shell structure, where the alginate encapsulated the collagen-MSC inner part was successfully generated. The fibrous hydrogel could be easily molded into any determined shape; a letter *DKU* using a prefabricated mold is shown as an example (Fig. 1c), indicating the tunability of the core–shell fibrous device to tissue defect 3D geometry.

Controlling the thickness of the core and shell part was possible by changing the alginate concentration and the injection speed, which could significantly affect the nutrient/oxygen penetration and the survival of cells encapsulated. Figure 2 shows the effect of these parameters on the shell and core thickness values. The shell thickness increased as the alginate concentration increased (from 200 μm at 2% alginate to 450 μm at 5% alginate, shown in Fig. 2a). The core thickness decreased at the highest alginate concentration (Fig. 2b).

The core–shell morphologies also reflected well the core and shell thickness change with respect to the alginate concentration (Fig. 2c–e). The effect of injection speed was also clearly seen; the shell thickness increased as the injection speed increased (from 100 μm at 20 mL/h to 400 μm at 80 mL/h; Fig. 2f), while the core thickness was not changed (Fig. 2g). The optical images also represent the core–shell thicknesses with varying the injection speed (Fig. 2h–j).

The mechanical properties of the core–shell hydrogel cell carrier were measured by DMA. Samples prepared with varying alginate concentrations were compared. Storage modulus (E') and loss modulus (E'') values recorded at different frequencies are shown in Figure 3. The storage modulus increased as the alginate concentration increased (from 30 kPa at 2% alginate to 50 kPa at 5% alginate; Fig. 3a), suggesting that an increasing alginate concentration improved the ability to withstand plastic deformation. The loss
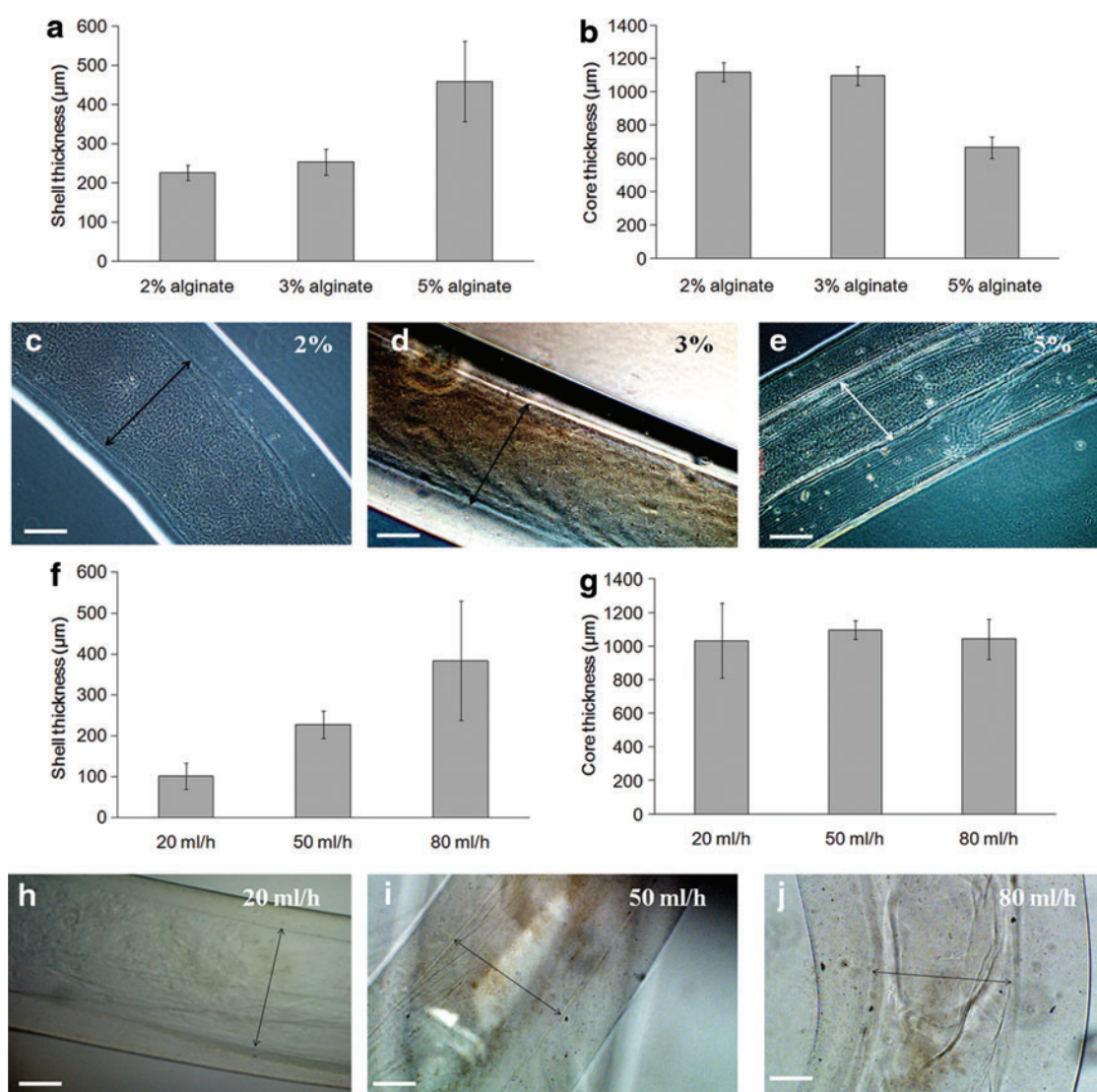

FIG. 2. Effect on alginate shell thickness of **(a–e)** alginate concentration and **(f–j)** injection speed. **(a)** Shell and **(b)** core thickness measured with respect to varying alginate concentrations. Optical images showing the core–shell fiber morphologies produced with different alginate concentrations; **(c)** 2%, **(d)** 3%, and **(e)** 5%. **(f)** Shell and **(g)** core thickness measured with respect to varying injection speed. Optical images showing the core–shell fiber morphologies produced with different injection speed; **(h)** 20, **(i)** 50, and **(j)** 80 mL/h. Arrows indicate the core thickness. Scale bars = 400 μm. Color images available online at www.liebertpub.com/tea
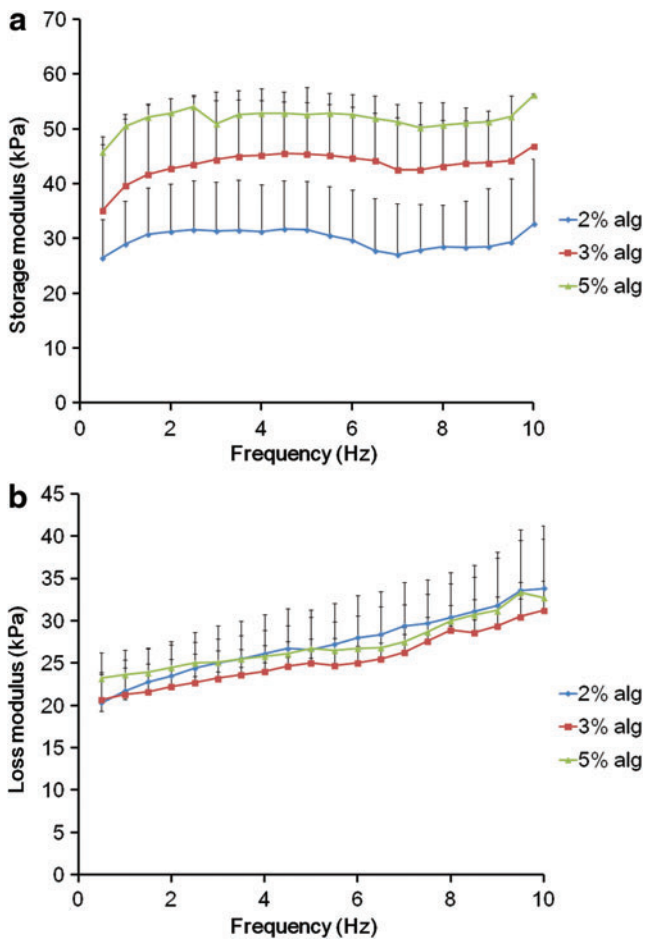
FIG. 3. Mechanical properties of the core–shell structured fibrous hydrogel cell carriers produced with different alginate concentrations (2%, 3%, and 5%), as measured by a dynamic mechanical analysis; **(a)** storage modulus and **(b)** loss modulus were recorded at varying frequency (from 0.1 to 10 Hz). Whereas storage modulus noticeably increased as alginate concentrations increased, not much change was observed in the loss modulus. Color images available online at www.liebertpub.com/tea

Table 1. Degradation of Core–Shell Fibrous Hydrogel Cell Carrier in Phosphate-Buffered Saline

Period in phosphate-buffered saline (days)	1	3	5	7	14
Degradation (%)	1.9	4.4	14.2	22.4	43.4

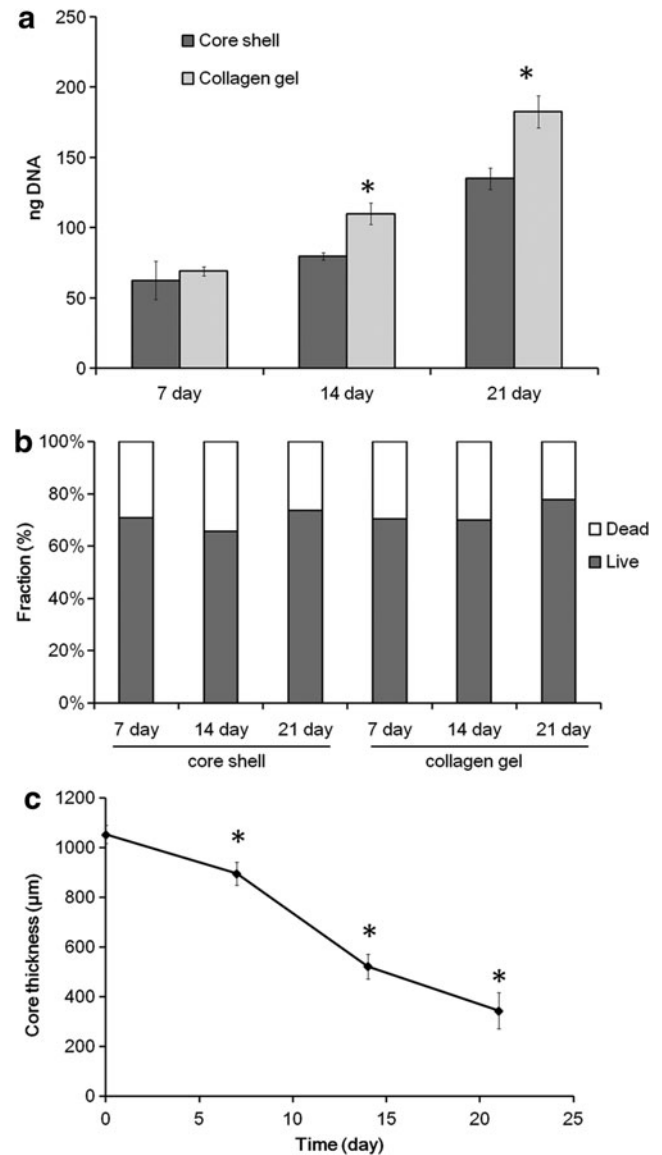Samples produced with 3% alginate were tested as the representative group.

FIG. 4. **(a)** Proliferation of MSCs within the core–shell fibrous hydrogel carrier over 21 days, as assessed by the DNA quantification. Results are compared with the MSCs cultured within collagen hydrogel used as a positive control. Cell proliferation comparable at 7 days became different at prolonged periods of 14 and 21 days (core–shell < collagen, *$p < 0.05$, statistically different). **(b)** Live/dead cells quantified for both groups by trypan blue screening and hemocytometer counting, showing comparable levels for both cases (~70% survival rate at all time points). **(c)** Collagen core shrinkage measured for up to 21 days, showing a considerable decrease in the core size from ~1050 μm (initial) to 900 μm at 7 days, 500 μm at 14 days, and 350 μm at 21 days.
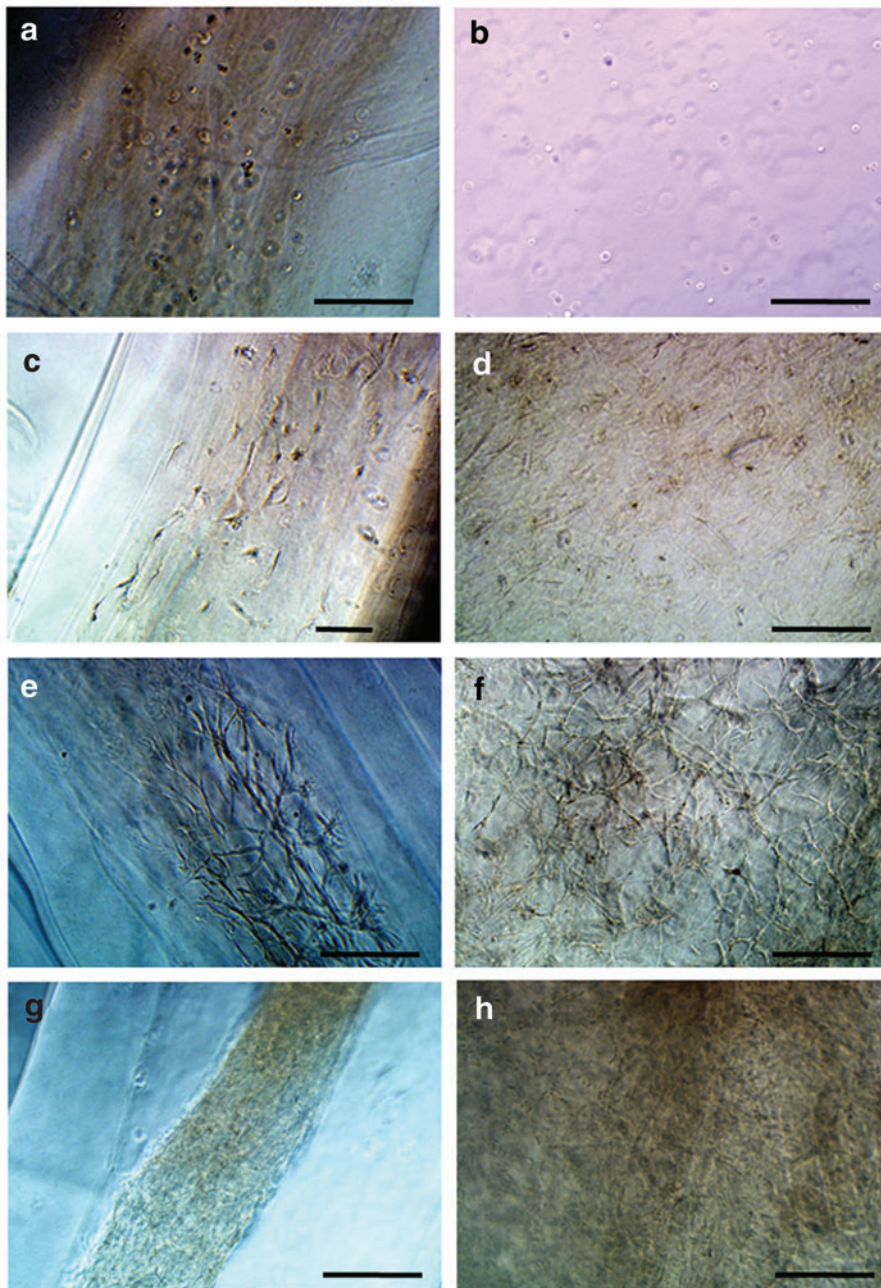
modulus presented very similar values for the different alginate concentrations (Fig. 3b), suggesting that the viscous behavior of the scaffolds was not affected by the alginate concentration. Whereas the storage modulus did not show close dependence on the frequency parameter, the loss modulus showed an almost linear increase as the frequency increased. Moreover, the storage modulus values recorded were higher than the loss modulus values for all cases.

Degradation of the core–shell hydrogel cell carrier was measured in PBS over 21 days. The cell carrier obtained with 3% alginate was tested as the representative group. Weight loss measured was ~4% after 3 days, ~22% after 7 days, and ~43% after 14 days (Table 1). Further, the cell carrier was shown to take up water as high as 98%, as taken from the weight change between the hydrogel and freeze-dried samples, demonstrating a typical characteristic of hydrogels.

MSC proliferation, morphology, and osteogenesis

The proliferative potential and viability of MSCs encapsulated in the core–shell hydrogel carrier were investigated.

FIG. 5. Optical microscopic images of the core–shell hydrogel carrier, encapsulating MSCs at different culture periods **(a, c, e, g)** and collagen gel control incorporating MSCs at the corresponding culture period **(b, d, f, h)**. MSCs with a round shape initially at the time of seeding **(a, b)**, became spindle shaped at 7 days **(c, d)**, and then highly elongated at 14 days **(e, f)**. At 21 days **(g, h)**, cells proliferated extensively to reach near confluence. Collagen core part in the core–shell carrier appeared to shrink substantially with increasing culture time. Scale bars = 350 μm. Color images available online at www.liebertpub.com/tea

Results were compared with the MSCs cultured within the collagen hydrogel matrix, which has been shown to be an effective 3D matrix for cell growth and population and thus used in this study as a positive control. From DNA analysis, MSCs were shown to actively proliferate for both groups with an on-going increase in the proliferation level over 21 days (Fig. 4a). Whereas the cell proliferation level was comparable during 7 days for both groups, the proliferation in the collagen became significantly higher than that in the core–shell design after 14 and 21 days. Live/dead cell assays revealed comparable levels for both the collagen and core–shell groups, with ~70% of cell viability at all culture periods (Fig. 4b). Figure 4c shows the shrinkage of the collagen core where MSCs populated and proliferated over 21 days. There was a considerable decrease in the core diameter from 1050 μm (initial) to 900 μm at 7 days, 500 μm at 14 days, and 350 μm at 21 days.

Figure 5 displays representative optical microscopy images of MSCs during culture for up to 21 days when encapsulated within the core–shell fibrous hydrogel carrier as well as those incorporated within collagen gel. MSCs initially displayed a round shape soon after encapsulation (Fig. 5a) and a number of cytoskeletal extensions were evident after 7 days of culture (Fig. 5c), which was similarly observed in the collagen gel control group (Fig. 5b, d). Cells in the core–shell carrier became highly elongated at day 14 (Fig. 5e). Interestingly, the cells showed directional elongation along the fiber axis. The cells in the collagen were also highly elongated, but randomly elongated (Fig. 5f). At 21 days, the cells in the core–shell carrier reached near confluence within the collagen core
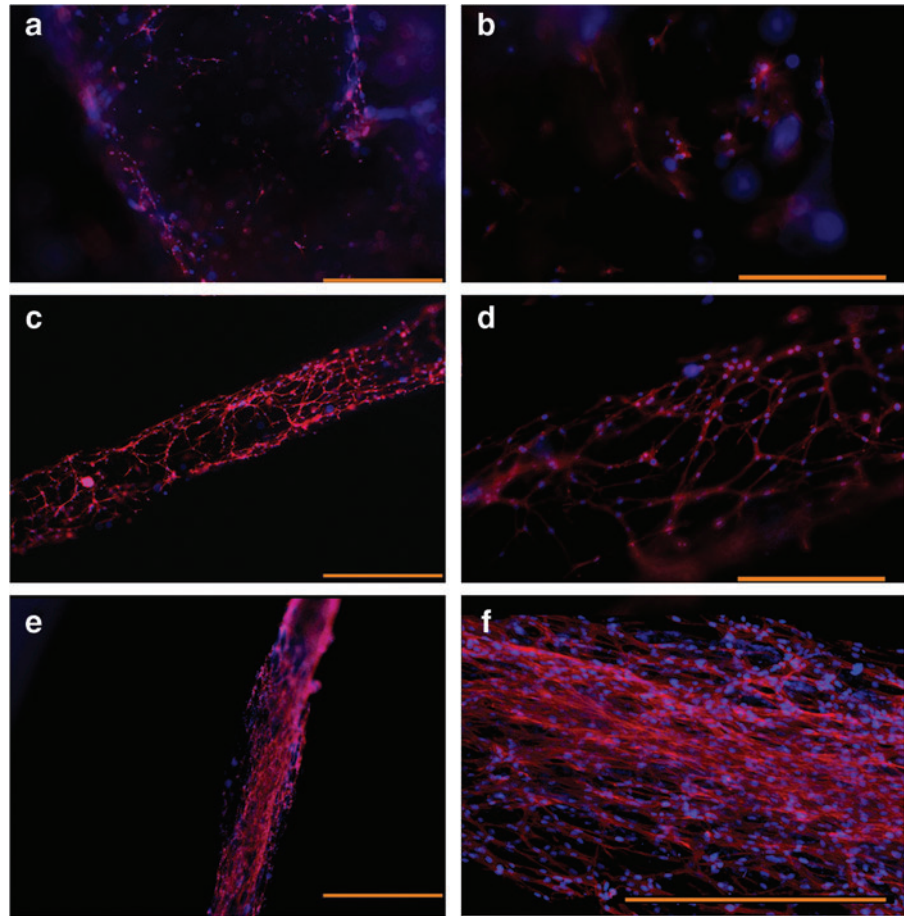
FIG. 6. Confocal laser scanning microscopy showing the cellular cytoskeletal processes and the elongation morphology within the core–shell fibrous carrier after 7 **(a, b)**, 14 **(c, d)**, and 21 days **(e, f)**. Cell nucleus stained in blue (4′,6-diami-dino-2-phenylindole) and the cyto-skeleton in red (Alexa Fluor Phalloidin 548). Scale bars = 850 μm **(a, c,** and **e)** and 350 μm **(b, d,** and **f)**. Color images available online at www.liebertpub.com/tea

(Fig. 5g), and a similar behavior was observed in the collagen gel (Fig. 5h). The collagen core part in the core–shell system appeared to shrink substantially at prolonged culture periods.

The cellular cytoskeletal process and elongation morphology were revealed after immunofluorescence staining of the cells and observation under confocal microscopy, as shown in Figure 6. MSCs with limited cytoskeletal extensions at day 7 (Fig. 6a, b) showed pronounced elongation, forming a highly networked structure among the cells at day 14 (Fig. 6c, d). The cell networks appeared to be formed primarily at the outer surface of the core part, that is, close to the core–shell boundary. Once cell confluence at the surface region was reached, cells grew and proliferated at the inner region of the collagen core part, and at day 21, cells formed more dense networks throughout the collagen core, which was highly oriented along the fiber axis (Fig. 6e, f).

The osteogenic differentiation of the MSCs cultured in the core–shell fibrous carrier was assessed in terms of expression of genes related with bone, including BSP, OPN, and OCN. Figure 7 shows the mRNA expression levels of those genes (expression levels presented by normalizing to collagen gel at 14 days) by qPCR analysis. After culture for 14 days, all genes were expressed at levels significantly higher in the core–shell carrier than in the collagen gel; fold increases were 1.6, 3.0, and 5.5, respectively, for BSP, OPN, and OCN. At 21 days, however, the difference was reduced.

In vivo *bone forming ability of the MSC delivery system*

The tissue compatibility and bone forming ability of the MSC-encapsulated core–shell hydrogel carrier was further assessed using a rat calvarium model. Three different groups were studied: core–shell carrier only, carrier with MSCs as encapsulated, and carrier with MSC encapsulation followed by osteogenic differentiation for 7 days. Throughout the 6-week study period, animals showed a good healing response without adverse tissue reactions and material toxicity, as well as there were no visible signs of internal inflammation on the harvested tissues. Bone regeneration was examined with μCT, as shown in Figure 8. The μCT constructed images revealed new bone formation (orange colored) within the defect region for the three groups (Fig. 8a). Different levels of bone regeneration from the defect margins were noted. Based on the μCT images, the percent bone volume, bone surface area, and bone surface density were quantified. Whereas the percent bone volume of the carrier only was ~13%, that of MSC-encapsulated carrier showed 25%, and the differentiated MSCs increased the bone volume as high as 45% (Fig. 8b). The bone surface area and bone surface density also showed the effectiveness of the carrier encapsulating MSCs with osteogenic differentiation (Fig. 8c, d).

New bone formation and defect closure were revealed again by histological views after HE and MT stains, as shown in Figure 9. All three groups showed good biocompatibility with no significant notice of inflammatory cells. HE
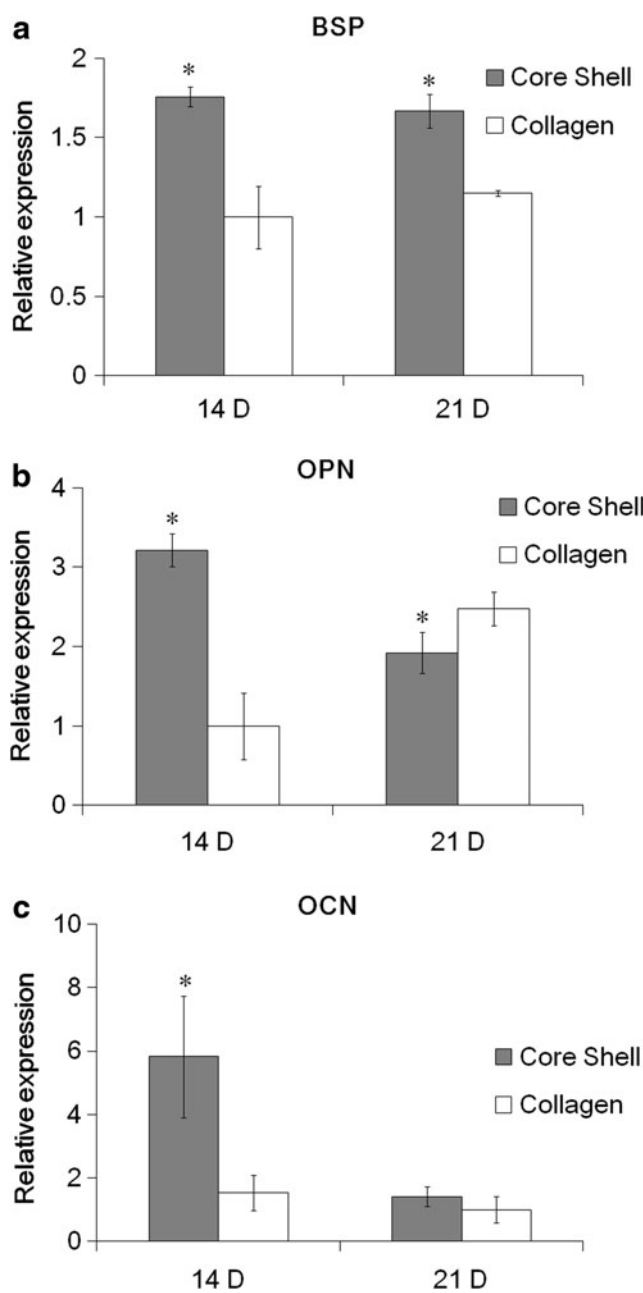
FIG. 7. Osteogenic differentiation of the MSCs cultured in the core–shell fibrous hydrogel carrier over 14 and 21 days. mRNA levels of bone sialoprotein (BSP) **(a)**, osteopontin (OPN) **(b)**, and osteocalcin (OCN) **(c)** genes were quantitatively assessed. * Indicates significant differences ($p < 0.05$, by analysis of variance).

FIG. 8. *In vivo* bone forming ability of the MSC-encapsulated core–shell hydrogel carrier. Three sample groups tested include carrier only (w/o cells), carrier with undifferentiated MSCs (nonosteogenic), and carrier with differentiated MSCs for 7 days in an osteogenic medium (osteogenic). Bone regeneration was analyzed by microcomputed tomography (μCT) after 6 weeks of implantation: **(a)** μCT constructed images showing the new bone formation (orange color) around the 5-mm-diameter defect region. Quantitative results showing **(b)** percent of new bone volume, **(c)** bone surface area, and **(d)** bone surface density. Significant differences were noticed (*$p < 0.05$ and **$p < 0.01$, by analysis of variance). Color images available online at www.liebertpub.com/tea

stains revealed cell and/or tissue in-growth within the defect region. MT stains showed more clearly the newly formed bone within the defect area. The carrier only group showed primarily loose connective tissue formed within the defect with a limited amount of new bone formation at the margin (Fig. 9a). In contrast, when undifferentiated MSCs were encapsulated within the carrier, a level of new bone formation (indicated as NB) was revealed at the center of defect (Fig. 9b). The group using carrier with differentiated MSCs showed a significant level of newly formed bone at the central reg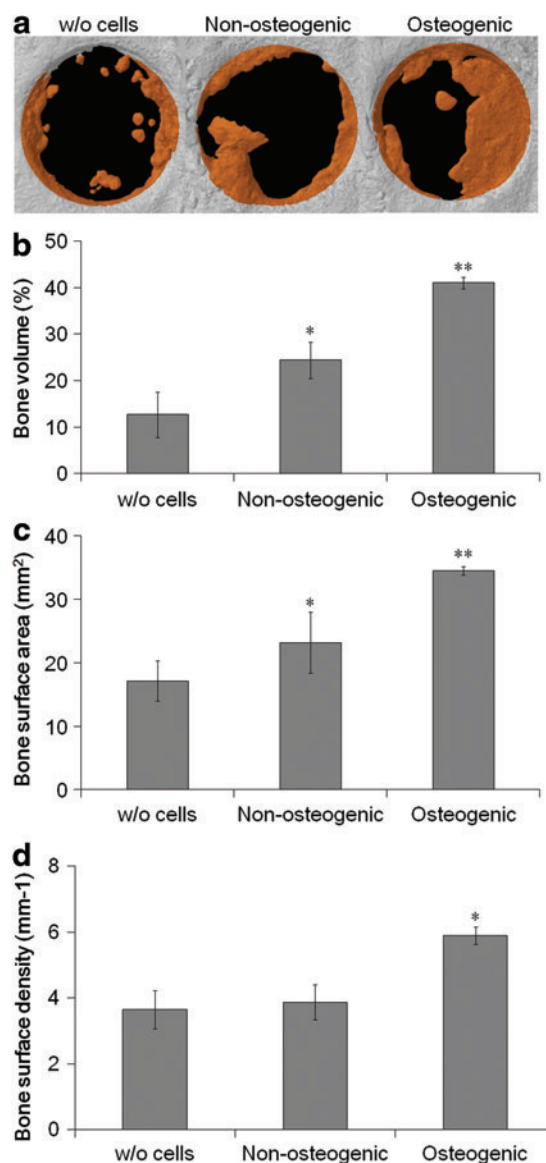ions of the defect (Fig. 9c). At higher magnification of the newly formed bone in Figure 9c, the new bone was proven to be mature with a compact structure and lined with many osteoblasts (Fig. 9d).

Discussion

Delivery of cells to tissue defect sites requires the use of appropriate 3D matrices that support the cell growth and are
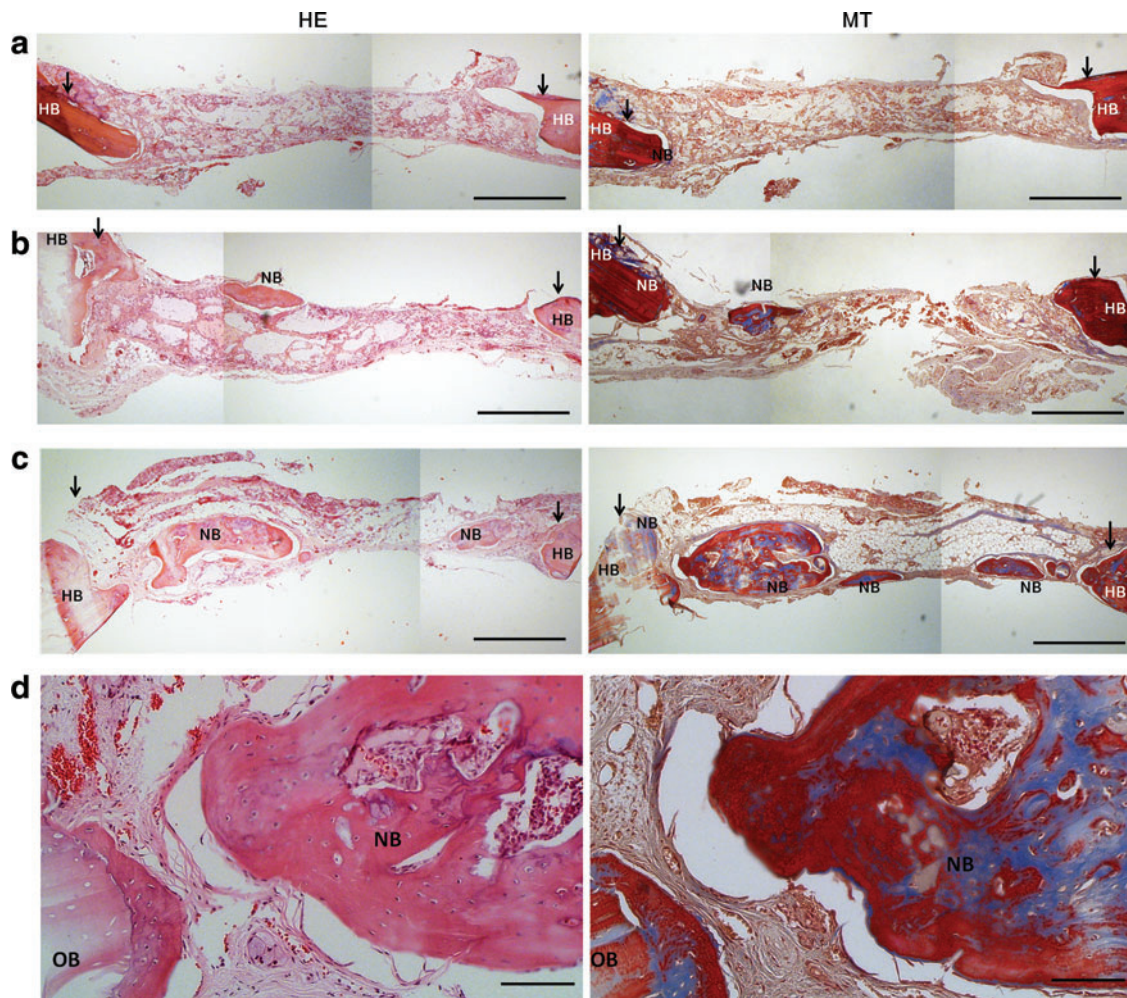
FIG. 9. Representative histological images of implanted samples after hematoxylin and eosin (HE) and Masson's trichrome (MT) staining after 6 weeks of implantation; **(a)** carrier only, **(b)** with undifferentiated MSCs, **(c)** with differentiated MSCs, and **(d)** enlarged image of newly formed bone in **(c)**. (Arrows: defect margins, NB: new bone, HB: host bone). Scale bar = 1 mm **(a–c)** and 200 μm **(d)**. Color images available online at www.liebertpub.com/tea

biologically compatible and even tunable to the defect shape. The cells loaded in the 3D matrices can be directly delivered to target defects, or cultured *ex vivo* to form a tissue-engineered construct that better mimics the native tissue structure and composition. Many types of 3D matrices have been developed to engineer and deliver cells to regenerate various tissues, including skin, bone, cartilage, nerve, and blood vessels.

In this study, a core–shell structured hydrogel system was designed as the 3D matrix for cell delivery. The hydrogel cell carrier was made of two clearly distinguished zones, an inner cell encapsulating collagen part ensheathed with an outer alginate. Specifically, the core–shell structure was generated into a fibrous morphology with diameters of hundreds of micrometers by directly depositing the solutions through a specially designed core–shell nozzle within a Ca-containing culture medium bath (Fig. 1). When the sodium (Na)-alginate meets the Ca ions, an ion exchange between Na and Ca occurs, resulting in the formation of divalent Ca crosslinks to the alginate and development of a hardened network of Ca-alginate outer shell.[18] Due to the rapid crosslinking of alginate, the cell-loaded collagen inner core could be main-

tained without loss of physical integrity. Because of these traits of the core–shell structured collagen-alginate hydrogel matrix, the water permeation and degradation properties are largely dependent on the outer alginate composition, particularly the hydrogel density.[18–20] Therefore, the core–shell fibers had to be carefully designed by selecting the appropriate speed of injection as well as the optimal alginate concentration to allow nutrient and oxygen diffusion to the cells in the core. It has been previously reported that, for hydrogels to allow cell survival, distances higher than 200–250 μm in the system may reduce oxygen transport as well as nutrient diffusion.[21] Thus, the core–shell system had to be designed for the shell thickness to lie within this range. It was observed that a high injection speed (80 mL/h) produced a thick shell inappropriate for encapsulating cells, while a low speed (20 mL/h) resulted in very slow scaffold processing with an increased risk of cell death during the *in situ* scaffold preparation (Fig. 2). Further, a high alginate concentration (5%) created a thicker and denser shell layer, possibly reducing the nutrient penetration, whereas a low concentration (2%) produced a similar layer to that of 3%, but with faster degradation and poorer mechanical

properties (Fig. 2). Therefore, an intermediate speed (50 mL/h) with an intermediate alginate concentration (3%) was selected for further cell encapsulation experiments.

To prove the ability of cells to survive in the designed scaffold, MSCs were encapsulated in the collagen and ensheathed with 3% alginate, and the cell proliferation and viability level were assessed in direct comparison with those loaded within pure collagen gel. MSCs exhibited high levels of viability, maintaining a proliferative potential comparable to the pure collagen hydrogel matrix (Fig. 4). Based on the optical cell images, as well as measurement of cell viability, including the live/dead cell count, the engineered core–shell collagen-alginate hydrogel delivery system provides appropriate 3D matrix conditions for cells to undergo a series of normal and favorable responses. Of particular note is the fact that the cells in the core–shell fibrous hydrogel exhibited preferential direction of growth along the fiber axis, whereas in the collagen gel, the orientation was random. Further, the cells were preferentially positioned in close proximity to the alginate, forming hollow cylindrical cellular networks (Figs. 5 and 6). It is thought that the encapsulated cells favor and thus migrate to the areas where the oxygen and nutrient levels are higher. Another finding is the shrinkage of the collagen inner core toward the central axis during the culture period, which is closely related with the high proliferation of cells. It is thus considered that the degradation of the core–shell hydrogel over culture period was primarily from the collagen degradation. Although the collagen inner core degraded to shrink a lot, cells proliferated substantially, forming a network along the fiber direction, and the whole core–shell fibrous morphology could be preserved due to the presence of a relatively stable alginate shell. This suggests that the designed core–shell fibrous system is sufficient for the cell delivering tissue engineering matrix, by encapsulating cells in an isolated, but nutrient and oxygen permissible environment and delivering them to target defects.

After addressing the cell viability and morphological traits, we further analyzed the osteogenic phenotype expression of the MSCs cultured within the core–shell delivery system (Fig. 7). A series of osteogenic genes (OPN, BSP, and OCN) were highly expressed at day 14, with levels significantly higher than those in pure collagen gel. Although the cell growth matrices are the same (collagen gel), the osteogenic development was differently processed. Some possible explanations can be given. First, the different morphological feature of cells (directional elongation vs. random spreading) will influence the MSC osteogenic differentiation. Similar effects have been previously found when cells were cultured on aligned polymer fibrous matrices.[22,23] Second, the confined core–shell matrix would provide different microenvironments for MSCs to undergo cellular processes, particularly osteogenic differentiation; the possible differences in cell-to-cell contact, secretion of endogenous signals, nutrient diffusion, and oxygen levels might be the cause.[24,25] However, further in-depth study is needed to elucidate which parameter is the most significant, and thus to optimize the MSC-loaded core microenvironments. It is further envisaged that the incorporation of signaling or osteogenic factors within the core or shell part is a promising strategy for exogenous regulation of stem cell functions.[26] Compositional change of the core material is another strategy to im-

prove the matrix properties for osteogenesis within the current design of the core–shell delivery system.

When the osteogenic development of MSCs was confirmed under *in vitro* culture, we next sought to find the efficacy of the MSC-delivering core–shell hydrogel system in the *in vivo* bone regeneration. Three experimental groups were tested in a rat calvarium defect for 6 weeks, which includes core–shell carrier only, carrier with MSCs undifferentiated, and carrier with MSCs differentiated for 7 days. In fact, the delivery system was very effective for handling and implantation, being easily formulated into the defects made in calvarium, which allows possible uses in more complex-shaped defect models. A first *in vivo* sign proved that the cell carrier system had good biocompatibility with no adverse tissue reaction or significant inflammation. Whereas the core–shell carrier group exhibited only a limited bone formation at the circumferential defect areas, the MSC-delivering groups showed bone regeneration at the central areas (Figs. 8 and 9). Moreover, when the MSCs delivered were differentiated into an osteogenic lineage, the bone ingrowth was more substantial. These results demonstrated the role of MSCs, particularly those engineered into an osteogenic lineage, in the *in vivo* bone regeneration, and the efficacy of the core–shell fibrous cell delivery system. The MSCs in the core–shell carrier secrete signaling molecules to the surrounding tissue allowing new bone formation, while preserving cellular integrity within the hydrogel carrier system. Based on this observation, the newly designed core–shell fibrous hydrogel is believed to have potential future applications as a stem cell delivering matrix and defect-tuned bone tissue engineering.

Conclusions

A collagen core-alginate shell fibrous hydrogel scaffold was designed for the delivery of cells and for tissue engineering of bone. The hydrogel scaffold was shown to provide 3D matrix conditions appropriate for MSCs to survive and proliferate, and to undergo osteogenic differentiation using appropriate chemical cues. Further, the MSCs delivered through hydrogel scaffolds showed great potential for regenerating bone tissue in a rat calvarium model. Taken together, the newly developed core–shell structured collagen-alginate system may be useful for tissue engineering and the delivery of stem cells in regeneration of damaged and degenerated bone tissues.

Acknowledgments

Disclosure Statement

No competing financial interests exist.

References

1. Arvidson, K., Abdallah, B.M., Applegate, L.A., Baldini, N., Cenni, E., Gomez-Barrena, E., Granchi, D., Kassem, M., Konttinen, Y.T., Mustafa, K., Pioletti, D.P., Sillat, T., and

Finne-Wistrand, A. Bone regeneration and stem cells. J Cell Mol Med **15,** 718, 2011.

2. Marolt, D., Knezevic, M., and Vunjak-Novakovic, G. Bone tissue engineering with human stem cells. Stem Cell Res Ther **1,** 10, 2010.

3. Perez, R.A., Won, J.E., Knowles, J.C., and Kim, H.W. Naturally and synthetic smart composite biomaterials for tissue regeneration. Adv Drug Deliv Rev **65,** 471, 2013.

4. McNamara, L.E., McMurray, R.J., Biggs, M.J.P., Kantawong, F., Oreffo, R.O.C., and Dalby, M.J. Nanotopographical control of stem cell differentiation. J Tissue Eng **2010,** 120623, 2010.

5. Ghidoni, I., Chlapanidas, T., Bucco, M., Crovato, F., Marazzi, M., Vigo, D., Torre, M.L., and Faustini, M. Alginate cell encapsulation: new advances in reproduction and cartilage regenerative medicine. Cytotechnology **58,** 49, 2008.

6. Sayyar, B., Dodd, M., Wen, J., Ma, S., Marquez-Curtis, L., Janowska-Wieczorek, A., and Hortelano, G. Encapsulation of factor IX–engineered mesenchymal stem cells in fibrinogen–alginate microcapsules enhances their viability and transgene secretion. J Tissue Eng **3,** 2041731412462018, 2012.

7. Zhang, J., Wang, Q., and Wang, A. *In situ* generation of sodium alginate/hydroxyapatite nanocomposite beads as drug-controlled release matrices. Acta Biomater **2,** 445, 2010.

8. Oh, S.A., Lee, H.Y., Lee, J.H., Kim, T.H., Jang, J.H., Kim, H.W., and Wall, I. Collagen three-dimensional hydrogel matrix carrying basic fibroblast growth factor for the cultivation of mesenchymal stem cells and osteogenic differentiation. Tissue Eng A **18,** 1087, 2012.

9. Wang, F., Li, Z., Khan, M., Tamama, K., Kuppusamy, P., Wagner, W.R., Sen, C.K., and Guan, J. Injectable, rapid gelling and highly flexible hydrogel composites as growth factor and cell carriers. Acta Biomater **6,** 1978, 2010.

10. Ferreira, A.M., Gentile, P., Chiono, V., and Ciardelli, G. Collagen for bone tissue regeneration. Acta Biomater **8,** 3191, 2012.

11. Orive, G., Hernandez, R., Gascon, A., and Pedraz, J.L. Encapsulation of cells in alginate gels. In: Guisan, J. Immobilization of Enzymes and Cells. Totowa, NJ: Humana Press, 2006, pp. 345–355.

12. Chayosumrit, M., Tuch, B., and Sidhu, K. Alginate microcapsule for propagation and directed differentiation of hESCs to definitive endoderm. Biomaterials **31,** 505, 2010.

13. Bohari, S.P.M., Grover, L.M., and Hukins, D.W.L. Pulsed-low intensity ultrasound enhances extracellular matrix production by fibroblasts encapsulated in alginate. J Tissue Eng **3,** 2041731412454672, 2012.

14. Chan, L.W., Lee, H.Y., and Heng, P.W.S. Production of alginate microspheres by internal gelation using an emulsification method. Int J Pharm **242,** 259, 2002.

15. Chan, L.W., Jin, Y., and Heng, P.W.S. Cross-linking mechanisms of calcium and zinc in production of alginate microspheres. Int J Pharm **242,** 255, 2002.

16. Bidarra, S.J., Barrias, C.C., Barbosa, M.A., Soares, R., and Granja, P.L. Immobilization of human mesenchymal stem cells within RGD-grafted alginate microspheres and assess-ment of their angiogenic potential. Biomacromolecules **11,** 1956, 2010.

17. Perez, R.A., and Kim, H.W. Core shell designed scaffolds of alginate/alpha-tricalcium phosphate for the loading and delivery of biological proteins. J Biomed Mater Res A **101,** 1103, 2013.

18. Augst, A.D., Kong, H.J., and Mooney, D.J. Alginate hydrogels as biomaterials. Macromol Biosci **6,** 623, 2006.

19. Bolewski, K. On the effect of ionic strength on the degradation of sodium alginate. Die Makromolekulare Chemie **66,** 1, 1963.

20. Pathak, T.S., Yun, J.H., Lee, J., and Paeng, K.J. Effect of calcium ion (cross-linker) concentration on porosity, surface morphology and thermal behavior of calcium alginates prepared from algae (*Undaria pinnatifida*). Carbohydr Polym **81,** 633, 2010.

21. Fidkowski, C., Kaazempur-Mofrad, M.R., Borenstein, J., Vacanti, J.P., Langer, R., and Wang, Y. Endothelialized microvasculature based on a biodegradable elastomer. Tissue Eng **11,** 302, 2005.

22. Ma, J., He, X., and Jabbari, E. Osteogenic differentiation of marrow stromal cells on random and aligned electrospun poly(l-lactide) nanofibers. Ann Biomed Eng **39,** 14, 2011.

23. Wang, Y., Gao, R., Wang, P.P., Jian, J., Jiang, X.L., Yan, C., Lin, X., Wu, L., Chen, G.Q., and Wu, Q. The differential effects of aligned electrospun PHBHHx fibers on adipogenic and osteogenic potential of MSCs through the regulation of PPARγ signaling. Biomaterials **33,** 485, 2012.

24. Zou, D., Zhang, Z., Ye, D., Tang, A., Deng, L., Han, W., Zhao, J., Wang, S., Zhang, W., Zhu, C., Zhou, J., He, J., Wang, Y., Xu, F., Huang, Y., and Jiang, X. Repair of critical-sized rat calvarial defects using genetically engineered bone marrow-derived mesenchymal stem cells over-expressing hypoxia-inducible factor-1α. Stem Cells **29,** 1380, 2011.

25. Tseng, W.P., Yang, S.N., Lai, C.H., and Tang, C.H. Hypoxia induces BMP-2 expression via ILK, Akt, mTOR, and HIF-1 pathways in osteoblasts. J Cell Physiol **223,** 810, 2010.

26. Wu, D.Q., Wang, T., Lu, B., Xu, X.D., Cheng, S.X., Jiang, X.J., Zhang, X.Z., and Zhuo, R.X. Fabrication of supramolecular hydrogels for drug delivery and stem cell encapsulation. Langmuir **24,** 10306, 2008.

Address correspondence to:
Hae-Won Kim, PhD
Institute of Tissue Regeneration Engineering (ITREN)
Dankook University
Cheonan 330-714
South Korea

E-mail: kimhw@dku.edu